Solid and liquid spectroscopic analysis (SALSA) – a soft x-ray spectroscopy endstation with a novel flow-through liquid cell

Authors:

M. Blum[1,2] *, L. Weinhardt[1] *, O. Fuchs[1], M. Bär[2,3], Y. Zhang[2], M. Weigand[1], S. Krause[1,2], S. Pookpanratana[2], T. Hofmann[2], W. Yang[4], J. D. Denlinger[4], E. Umbach[1,5], and C. Heske[2] *

[1] *Universität Würzburg, Experimentelle Physik II, Am Hubland, 97074 Würzburg, Germany*

[2] *Department of Chemistry, University of Nevada, Las Vegas, 4505 Maryland Pkwy., Las Vegas, NV 89154-4003, USA*

[3] *Helmholtz-Zentrum Berlin für Materialien und Energie, Glienicker Str. 100, 14109 Berlin, Germany*

[4] *Advanced Light Source, Lawrence Berkeley National Laboratory, 1 Cyclotron Road, Berkeley, CA 94720, USA*

[5] *Karlsruhe Institute of Technology and Forschungszentrum Karlsruhe, 76021 Karlsruhe, Germany*

* To whom correspondence should be addressed: Monika.Blum@physik.uni-wuerzburg.de, phone: +49 931 888 5742, Lothar.Weinhardt@physik.uni-wuerzburg.de, phone: +49 931 31 83570, heske@unlv.nevada.edu, phone +1 702 895 2694

Abstract:

We present a novel synchrotron endstation with a flow-through liquid cell designed to study the electronic structure of liquids using soft x-ray spectroscopies. In this cell, the liquid under study is separated from the vacuum by a thin window membrane, such that the sample liquid can be investigated at ambient pressure. The temperature of the probing volume can be varied in a broad range and with a fast temperature response. The optimized design of the cell significantly reduces the amount of required sample liquid and allows the use of different window membrane types necessary to cover a broad energy range. The liquid cell is integrated into the SALSA (**S**olid **A**nd **L**iquid **S**pectroscopic **A**nalysis) endstation that includes a high-resolution, high-transmission x-ray spectrometer and a state-of-the-art

electron analyzer. The modular design of SALSA also allows the measurement of solid-state samples. The capabilities of the liquid cell and the x-ray spectrometer are demonstrated using a RIXS (resonant inelastic x-ray scattering) map of a 25 wt% NaOD solution.

1. Introduction

In recent years, the investigation of the electronic structure of liquids has grown to a vivid research field. While *structural* information has been available for a long time ([1, 2, 3] and references therein), the study of the *electronic* structure of liquids is a technical challenge. The techniques commonly used for the investigation of the electronic structure of solid-state samples, in particular photoelectron spectroscopy (PES) as well as soft x-ray emission (XES) and absorption (XAS) spectroscopy, require ultra-high vacuum (UHV), which seems to be incompatible with liquid samples. Nevertheless, these techniques offer a wealth of information about the electronic and chemical structure, and thus first attempts to study liquids (with PES) date back to the early seventies [4]. Today, such PES studies have evolved into experiments using a sophisticated liquid micro jet injected directly into the vacuum [5, 6, 7]. In such experiments, the liquid is, however, far away from thermodynamic equilibrium and, due to the short inelastic mean free path of the electrons (typically a few nanometers), only the surface of the liquid can be studied (which in generally is different from the bulk [8]). Other approaches use hard x-ray excitation, e.g., for XAS, Raman-type absorption spectroscopy, and high-energy PES, but substantial limitations regarding chemical specificity and/or spectral resolution exist for most techniques and experimental set-ups.

Such limitations can be overcome by using XES and XAS (the latter in fluorescence yield mode). Compared to PES, these photon-in-photon-out techniques exhibit a much higher information depth (a few hundred nanometers in most cases) and are thus bulk-sensitive. Furthermore, the liquid sample can then be separated from the vacuum by a thin (100 – 1000

nm) membrane and confined to a “liquid cell”, which makes it possible to study the liquid in thermodynamic equilibrium at normal pressure.

The first XES and XAS experiments on liquids were performed using static liquid cells [9, 10, 11, 12]. In a static cell, a small amount of liquid is encapsulated behind a window membrane on a modified sample holder, which allows the introduction of the liquid cell into UHV like any other (dry) solid sample. However, there are several disadvantages of the static cell concept. First, a temperature control with this design is difficult and was not implemented in any of these early static cells. Furthermore, due to the (necessary) high x-ray intensity for XES measurements, an increased local temperature in the liquid near the window membrane is unavoidable, even when the liquid cell body is externally cooled. For water and many other liquids, this can lead to the formation of bubbles behind the window. Dissociation processes can also lead to gas formation and to rapid beam damage of dissolved molecules in the liquid or even of solvent molecules. Furthermore, solutions generally suffer from the deposition of solutes (or fragments thereof) on the inside of the membrane, which can have a strong contribution to the measured spectra. And, finally, chemical interactions between the liquid and the window membrane can occur, e.g., the oxidation of (oxygen-free) Si-based membranes during the study of water [13].

To avoid these issues we have recently published the description of a flow-through liquid cell [13]. This cell is integrated into a standard UHV sample manipulator with XYZ-translation. In this design, the investigated liquid is continuously sucked through the cell, such that the flow rate of the liquid is approximately 45 µl/s, e.g., replacing the content of the cell 15 times per second. Due to this improvement, reliable XES data on liquid water can now be collected, avoiding all of the above-discussed shortcomings of static cells [14, 15]. Furthermore, experiments on larger molecules (e.g., amino acids) in solution are possible without beam damage. A similar design of a flow-through cell is used by Forsberg et al. [16] to study atmospheric corrosion by soft x-rays.

By using the new set-up, we are preparing the investigation of biologically relevant systems in native environment. Therefore, we want to integrate an optical microscope into the liquid cell. Also, improved temperature control is desirable, and further applications (such as *in-situ* chemical bath deposition and electrochemical cells) required a complete re-design, such that the cell is easily accessible from the outside and not incorporated into a UHV manipulator. Thus, we have developed a new flow-through liquid cell, which will be presented in this paper.

The new cell is part of a synchrotron endstation dedicated to the study of liquids and solids, which includes a custom-designed analysis chamber and a high-resolution high-transmission soft x-ray spectrometer [17] in addition to a state-of-the-art electron spectrometer. After describing the liquid cell design in Section 2, this endstation will be described in Section 3 of this paper. First results obtained with the experimental setup will be shown in Section 4.

2. Flow-through liquid cell –design and advantages

Figure 1 shows an exploded view of the new liquid flow-through cell. The cell is integrated into a standard CF150 (8" outer diameter) blank flange. Its "heart" is a removable inset which is vacuum-sealed with a Viton O-ring. The inset contains the window membrane, also sealed with a Viton O-ring, a stainless steel plate with two feedthroughs (inlet and outlet), and a channel for the liquids. This is depicted in Fig. 2, which shows a detailed sketch of the inset. The sample liquid is sucked through the inlet into a 100 μm deep channel (65 mm long and 1.3 mm wide) and passes behind the window membrane, creating a bubble-free laminar flow. With respect to the previous design [13], the liquid volume in the cell is reduced from 15 to 8.5 μl. It can be separated from the liquid reservoir by fast-closing liquid valves (Parker; see Fig. 1). In the case of a membrane rupture, a fast pressure sensor closes the valves within 1.5 ms, leaving only the small liquid volume of the liquid cell exposed to the vacuum. Furthermore, the overall sample volume is minimized by the out-of-vacuum design. Due to

the easy accessibility of the liquid valves, all tubes are outside the vacuum and can be kept very short. Thus, the minimal total volume required for the liquid sample is reduced to less than 10 ml.

One big advantage with respect to the older design is the easy and fast exchange of the inset and the possibility to use very different membrane types (i.e., materials), sizes, and thicknesses by having insets adapted to the respective membrane. The different membrane types are important to optimize the transmission for the absorption edges under study. Since the focus of our experiments is on organic samples, the most important edges are the oxygen K, carbon K, nitrogen K, and sulfur $L_{2,3}$ edges. There are two requirements for a suitable membrane material: First, the membrane must not contain the studied element and second, the transmission should be high at the respective absorption edge. Therefore, we use Si_3N_4 membranes (Silson) with a thickness of ~100 nm for the O K and the C K edge measurements, and SiC membranes (NTT) with a thickness of ~150 nm for the N K edge. Due to the strong absorption of the Si $L_{2,3}$ edge, both membrane materials are not suited for measurements at the S $L_{2,3}$ edge, since the theoretical transmission of both windows is below 1% [18]. Instead, carbon-based (and Si-free) materials can be used [10].

For temperature-controlled measurements, a separate, Teflon-insulated liquid circuit channel is milled into the flange around the inset (see Fig. 1), allowing us to vary the temperature in the cell between 1°C and 90°C. A temperature control liquid is pumped through the channel by a water chiller, resulting in a very fast temperature response. The new flexible cell design can be used for a variety of different experiments, using different insets for variable membrane types as well as an inset for solid state samples. The latter is important to obtain reference spectra for comparison with the liquids. Furthermore, it is possible to perform optical microscopy of the liquid sample exposed to the beam. For the latter, the stainless steel plate containing the liquid channel is replaced by a glass plate, and a microscope is mounted between the fast-closing liquid valves (see Fig. 1).

3. The SALSA Endstation – home of the flow-through liquid cell

The SALSA ("**S**olid **A**nd **L**iquid **S**pectroscopic **A**nalysis") endstation with the mounted liquid cell is shown in Fig. 3a. SALSA includes a custom-built analysis (vacuum) chamber (with the attached flow-through liquid cell), a high-resolution high-transmission x-ray spectrometer described in more detail below and in [17], and a Specs PHOIBOS 150MCD electron analyzer. For solid sample measurements the cell can be replaced by a custom-built preparation chamber with a standard UHV manipulator and surface preparation equipment, as discussed below (Fig. 3b shows a photograph of SALSA with the mounted preparation chamber).

The CF150 flange of the new flow-through liquid cell is attached to the backside of the analysis chamber (see inset Fig. 3a). It is connected to the chamber via a CF150 pneumatic valve (VAT) with an independent pumping system. With this valve the flow-through liquid cell can be separated from the analysis chamber, which is useful for two reasons. First, with the valve closed it is possible to replace the inset or the membrane without compromising the vacuum in the SALSA analysis chamber. Second, it protects the analysis chamber in the case of a membrane rupture. In this case, sample liquid is released into the vacuum leading to a fast pressure rise in the chamber. At a pressure of 5×10^{-7} mbar, a fast pressure sensor trips, closing not only the fast liquid valves in the cell, but also the CF150 pneumatic valve, a CF40 pneumatic valve separating the analysis chamber and the soft x-ray spectrometer, and a fast valve installed in the beamline close to the endstation.

The analysis chamber is nearly a semi-cylinder, with the center point at the window membrane of the liquid cell. This center point is also the focus position of the synchrotron beam and the x-ray and electron spectrometers. To achieve this alignment, the entire analysis chamber can be adjusted with micrometer precision using an xyz-stage (Huber). The range of motion is ±25 mm in the x and y direction and 10 mm in the z direction, respectively.

The soft x-ray spectrometer is attached to the analysis chamber with a bellow, and thus it maintains its position with respect to the synchrotron beam when the analysis chamber is moved to align the liquid cell to the beam. The high-resolution, high-transmission spectrometer [17] uses the refocused synchrotron spot on the sample as source (≤30 μm), alleviating the need for an entrance slit. Furthermore, it contains a spherical mirror, a subsequent plane blazed variable-line-space (VLS) grating, and an uncoated back-illuminated CCD-camera detecting the photons in normal incidence. Our VLS spectrometer is optimized for all biological relevant edges (O K, N K, C K, S $L_{2,3}$) in one energy window with a resolving power of $E/\Delta E > 1200$ over the whole energy range (130 to 650 eV). It reaches an efficiency about two orders of magnitude higher than other state-of-the-art spectrometers, which allows the collection of an entire set of resonant x-ray emission spectra with variable excitation energy within less than an hour. Such a set can then be presented as a "RIXS map", as will be demonstrated in Section 4 below. Further detailed information about the VLS spectrometer and other RIXS maps can be found in [15, 17, 19, 20].

SALSA is – as the name tells – not only an endstation for liquids but also for solid state samples. As mentioned above, a preparation chamber with a standard manipulator can be attached to the back of the analysis chamber, replacing the flow-through liquid cell (Fig. 3b). Furthermore, an electron analyzer (SPECS Phoibos 150 MCD) is installed in the analysis chamber. Since the analyzer is rigidly attached and thus has to be moved with the entire chamber, the analyzer is suspended with six springs to remove the load from the chamber and, in particular, the xyz-stage.

4. SALSA in action: XAS and RIXS map of an NaOD solution

In the recent past, XES and XAS experiments on liquids mainly focused on the investigation of liquid water [3, 12, 14, 21, 22]. Especially the local hydrogen bond configuration was and still is under discussion [14, 15, 22, 23]. Fuchs et al. [14] and Tokushima et al. [22] presented

new high-resolution XES (HRXES) spectra that reveal a fine structure in the $1b_1$ emission line of liquid water. Furthermore, a surprisingly large isotope effect between the H_2O and D_2O XES spectra was observed, as well as temperature and excitation-energy dependence. In our model [14], the spectra are described as a superposition of two individual spectral components, one representing the intact water molecules and the second one related to ultrafast molecular dissociation on the timescale of the emission process. The assignment of the latter component representing the dissociated water molecules is supported by its similarity to the (resonantly excited) XES spectrum of the OH^- ions in an aqueous sodium hydroxide (NaOH) solution, as well as theoretical considerations [12, 24, 25].

In this paper, we present the resonant inelastic x-ray scattering (RIXS) map of sodium deuteroxide (NaOD, 25 wt%) in a D_2O (deuterium oxide, also known as "heavy water") solution ("aqueous NaOD") to demonstrate the performance of the new flow-through liquid cell and the SALSA endstation. All measurements were performed at Beamline 8.0.1 of the Advanced Light Source (ALS) in Berkeley, CA.

First, Fig. 4 shows an O K-edge XAS spectrum of liquid D_2O (solid line) and aqueous NaOD (dotted line). The D_2O spectrum exhibits the typical water pre-edge at ~535 eV [12, 14, 26]. In the spectrum of aqueous NaOD, a "pre-pre-edge" at ~533 eV can additionally be observed. This pre-pre-edge is exclusively assigned to OD^- ions [27].

Fig. 5 shows the full RIXS map of aqueous NaOD. A RIXS map is a two-dimensional representation of the color-coded emission intensity as a function of emission (abscissa) and excitation (ordinate) energy. The emission spectrum at a (non-resonant) excitation energy of 549.9 eV is shown at the top of the map, and the spectrum on the right represents a partial (515.8 - 532.8 eV) fluorescence yield absorption spectrum (which is also shown in Fig. 4). The elastically scattered peak (Rayleigh line) can be found as a bright diagonal line with equal excitation and emission energies on the lower right corner of the map. The map can be separated into two main parts, namely below and above the absorption onset of D_2O (yellow

horizontal line in Fig. 5). Below this onset, the emission spectra (i.e., horizontal cuts through the RIXS map) are dominated by the two main peaks of the occupied OD^- ion orbitals (also shown in Fig. 6 for an excitation energy of 533 eV), namely the 3a and the $1e_1$ orbital (C_∞ point group). Above the D_2O absorption onset, four peaks are found, similarly to the emission spectrum of D_2O [14, 19, 22], consisting of emission from $1b_2$, $3a_1$, and (split) $1b_1$ orbitals. However, the presence of OD^- ions in the solution leads to some differences compared to the pure D_2O spectrum. In particular, the split in the $1b_1$ peak is not as evident as in the spectrum of pure D_2O. The high energy $1b_1$ component (which is assigned to undissociated heavy water molecules [14, 24, 25]) merely appears as a shoulder of the (dominant) low energy $1b_1$ peak. The vertical lines in Fig. 5 show the energetic positions of the emission lines from the different OD^- (red) and D_2O (black) orbitals.

As we will discuss in the following, the RIXS map approach allows us derive an undisturbed spectrum of OD^-. For this purpose, we choose an excitation energy between the absorption onset of OD^- (531.9 eV) and D_2O (533.3 eV). In this region, the emission spectra of OD^- are not influenced by emission from the D_2O molecules. Furthermore, we find a dispersing Raman-like regime at and below the OD^- absorption edge (hard to see but indicated by the dashed line in Fig. 5). Thus, we have chosen an excitation energy of 533 eV for a detailed discussion of the OD^- spectrum, which is above the Raman-regime but still below the D_2O absorption onset. The emission spectrum at this energy is shown in Fig. 6; as mentioned, two main peaks can be observed. The presence of two lines, as well as their energy separation, agrees well with our B3LYP/6-31G+(d,p) density functional theory calculations of a single (i.e., gas phase) OD^- ion.

In Fig. 6 the 3a orbital is found at an emission energy of 522.8 eV, and the $1e_1$ orbital at an emission energy of 526.3 eV, i.e., a separation of 3.5 eV. In comparison the calculated energy separation is found to be 3.3 eV. Furthermore, both peaks show a slight asymmetry on the low energy side. This asymmetry might be the result of different effects. First, the asymmetry

could be due to the limited excitation resolution which might result in contributions from the above-described Raman-regime. Second, the asymmetry might be attributed to different local environments of the individual OD^- ions with slightly different emission energies. Third, vibrational broadening might play a role. And finally, an ultra-fast dissociation on the same timescale as the RIXS process might be present, similar to the case of H_2O and D_2O. The exact origin of this asymmetry will be the subject of further investigations.

5. Summary

We have presented a novel flow-through cell designed to study the electronic structure of liquids using soft x-ray spectroscopies. The design is optimized to achieve a steady bubble-free flow of the liquid. At the same time, it minimizes the liquid volume and allows easy access to all functional parts of the cell from outside the ultra-high vacuum. It has a separate cooling/heating circuit offering a broad temperature range (1°C - 90°C) with a short response time.

The flow-through cell is integrated in the described SALSA endstation, which consists of an analysis chamber equipped with a high-resolution and high-transmission soft x-ray spectrometer and a state-of-the-art electron analyzer. Apart from the liquid samples, it is possible to measure solid state samples by replacing the flow-through cell by a preparation chamber and a standard sample manipulator.

The performance of the flow-through cell, the endstation, and the x-ray spectrometer is exemplarily demonstrated by a RIXS map of an NaOD solution (25 wt%), which can be interpreted by a superposition of OD^- and D_2O contributions with varying spectral weight as a function of excitation energy.

Acknowledgment

This work was supported by the German BMBF (projects No. 05 KS4WWA/6 and 05 KS4VHA/4). M. Blum acknowledges the support by the Stiftung der Deutschen Wirtschaft and M. Bär the support by the Emmy-Noether-Programm of the Deutsche Forschungsgemeinschaft. The Advanced Light Source is supported by the U.S. DOE under contract No. DE-AC02-05CH11231.

References

[1] B. Tomberli, C. J. Benmore, P. A. Egelstaff, J. Neuefeind, and V. Honkimäki, J. Phys. Condens. Matter **12**, 2597 (2000).

[2] R. T. Hart, C. J. Benmore, J. Neuefeind, S. Kohara, B. Tomberli, P. A. Egelstaff, Phys. Rev. Lett. **94**, 047801 (2005).

[3] Ph. Wernet, D. Nordlund, U. Bergmann, M. Cavalleri, M. Odelius, H. Ogasaware, L. Å. Näslund, T. K. Hirsch, L. Ojamäe, P. Glatze, L. G. M. Pettersson, and A. Nilsson, Science **304**, 995 (2004).

[4] H. Siegbahn and K. Siegbahn, J. Electron Spectrosc. Relat. Phenom **2**, 319 (1973).

[5] K. R. Wilson, B. S. Rude, J. Smith, C. Cappa, D. T. Co, R. D. Schaller, M. Larsson, T. Catalano, and R. J. Saykally, Rev. Sci. Instrum. **75**, 725 (2004).

[6] B. Winter and M. Faubel, Chem. Rev. **106**, 1176 (2006).

[7] M. Saes, F. v. Mourik, W. Gawelda, M. Kaiser, M. Chergui, Ch. Bressler, D. Gromlimund, R. Abela, Th. E. Glover, Ph. A. Heimann, R. W. Schoenlein, S. L. Johnson, A. M. Lindenberg, and R. W. Falcone, Rev. Sci. Instrum. **75**, 24 (2004).

[8] H. Siegbahn, J. Phys. Chem. **89**, 897 (1985).

[9] J.-H. Guo, Y. Luo, A. Augustsson, J.-E. Rubensson, C. Såthe, H. Ågren, H. Siegbahn, and J. Nordgren, Phys. Rev. Lett. **89**, 137402 (2002).

[10] C. Heske, U. Groh, O. Fuchs, L. Weinhardt, E. Umbach, T. Schedel-Niedrig, C. H. Fischer, M. C. Lux-Steiner, S. Zweigart, T. P. Niesen, F. Karg, J. D. Denlinger, B. Rude, C. Andrus, and F. Powell, J. Chem. Phys. **119**, 10467 (2003).

[11] L.C. Duda, T. Schmitt, A. Augustsson, and J. Nordgren, J. Alloys Compd. **362**, 116 (2004).

[12] M. Odelius, H. Ogasawara, D. Nordlund, O. Fuchs, L. Weinhardt, F. Maier, E. Umbach, C. Heske, Y. Zubavichus, M. Grunze, J. D. Denlinger, L. G. M. Pettersson, and A. Nilsson, Phys. Rev. Lett. **94**, 227401 (2005).

[13] O. Fuchs, F. Maier, L. Weinhardt, M. Weigand, M. Blum, M. Zharnikov, J. D. Denlinger, M. Grunze, C. Heske, and E. Umbach, Nucl. Instrum. Meth. A **585**, 172 (2008).

[14] O. Fuchs, M. Zharnikov, L. Weinhardt, M. Blum, M. Weigand, Y. Zubavichus, M. Bär, F. Maier, J. D. Denlinger, C. Heske, M. Grunze, and E. Umbach, Phys. Rev. Lett. **100**, 027801 (2008).

[15] O. Fuchs, M. Zharnikov, L. Weinhardt, M. Blum, M. Weigand, Y. Zubavichus, M. Bär, F. Maier, J. D. Denlinger, C. Heske, M. Grunze, and E. Umbach, Phys. Rev. Lett. **100**, 249802 (2008).

[16] J. Forsberg, L.-C. Duda, A. Olsson, T. Schmitt, J. Andersson, J. Nordgren, J. Hedberg, C. Leygraf, T. Aastrup, D. Wallinder, and J.-H. Guo, Rev. Sci. Instr. **78**, 083110 (2007).

[17] O. Fuchs, M. Blum, M. Weigand, E. Umbach, L. Weinhardt, M. Bär, C. Heske, J. D. Denlinger, Y.-D. Chuang, W. McKinney, Z. Hussain, E. Gullikson, M. Jones, P. Batson, and R. Follath, Rev. Sci. Instr. **80**, 063103 (2009).

[18] http://henke.lbl.gov/optical_constants/filter2.html

[19] L. Weinhardt, O. Fuchs, M. Blum, M. Bär, M. Weigand, J.D. Denlinger, Y. Zubavichus, M. Zharnikov, M. Grunze, C. Heske, and E. Umbach, J. Electron Spectrosc. Rel. Phenom., doi: 10.1016/j.elspec.2009.02.014 (2009).

[20] L. Weinhardt, O. Fuchs, A. Fleszar, M. Bär, M. Blum, M. Weigand, J. D. Denlinger, W. Yang, W. Hanke, E. Umbach, and C. Heske, Phys. Rev. B **79**, 165305 (2009).

[21] J. D. Smith, C. D. Cappa, K. R. Wilson, B. M. Messer, R. C. Cohen, and R. J. Saykally, Science **306**, 851 (2004).

[22] T. Tokushima, Y. Harada, O. Takahashi, Y. Senba, H. Ohashi, L. G. M. Pettersson, A. Nilsson, and S. Shin, Chem. Phys. Lett. **460**, 387 (2008).

[23] L. G. M. Pettersson, T. Tokushima, Y. Harada, O. Takahashi, S. Shin, and A. Nilsson, Phys. Rev. Lett. **100**, 249801 (2008).

[24] M. Odelius, Phys. Rev. B **79**, 144204 (2009).

[25] M. Odelius, J. Phys. Chem. A **113**, 8176 (2009).

[26] M. Cavalleri, M. Odelius, D. Nordlund, A. Nilsson, and L. G. M. Pettersson, Phys. Chem. Chem. Phys. **7**, 2854 (2005).

[27] C. D. Cappa,| J. D. Smith, B. M. Messer, R. C. Cohen, and R. J. Saykally, J. Phys. Chem. A **111**, 4776 (2007).

Figure captions:

Fig. 1 (note: the figure should be two columns wide): Exploded view of the flow-through liquid cell. For better visibility, the viton gaskets are not shown.

Fig. 2: Detailed sketch of the liquid cell inset and the plate with the liquid channel. The plate fits into the cut-out of the inset.

Fig. 3a: Picture of the SALSA endstation at Beamline 8.0.1 of the Advanced Light Source, Lawrence Berkeley National Lab. 1: analysis vacuum chamber, 2: CF150 flange with flow-through liquid cell (also shown in inset), 3: pneumatic valve to separate liquid cell and analysis chamber, 4: micrometer x-y-z precision stage, 5: VLS soft x-ray spectrometer, and 6: electron analyzer (Specs PHOIBOS 150MCD), suspended with springs.
3b: Picture of the SALSA endstation with connected standard manipulator for solid state samples.

Fig. 4: O K-edge XAS spectra of liquid D_2O (solid line) and NaOD solution 25 wt% (dotted line). The vertical lines represent the absorption onsets: D_2O at 533.3 eV and NaOD at 531.9 eV.

Fig 5: O K-edge RIXS map of an aqueous NaOD solution (25 wt%). The horizontal axis represents the emission energy, the vertical axis shows the excitation energy, and the emission intensity is color-coded (in arbitrary units). The absorption onset of D_2O is shown as yellow horizontal line. The vertical lines give the positions of the OD^- (red) and D_2O (black) orbitals. The Raman-regime is indicated by a dashed line. Above the map, a non-resonant spectrum at an excitation energy of 549.9 eV is shown. The right panel corresponds to a partial fluorescence yield absorption spectrum by integrating over all emission energies shown.

Fig. 6: O K-edge XES spectrum of an aqueous NaOD solution (25 wt%) at an excitation energy of 533.0 eV. The occupied orbitals of OD^- as calculated by density functional theory are shown at the respective emission lines.

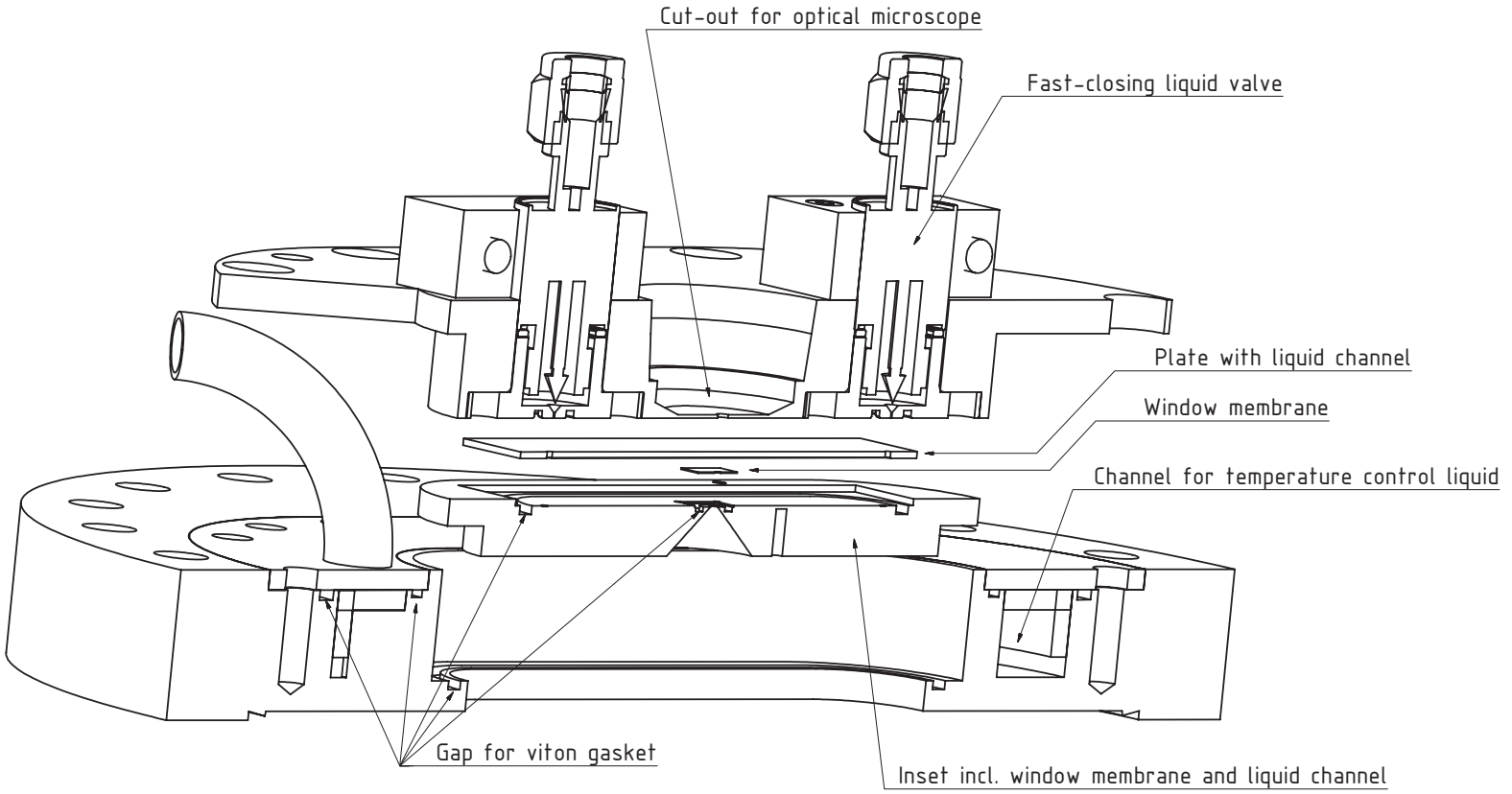
Cut-out for optical microscope
Fast-closing liquid valve
Plate with liquid channel
Window membrane
Channel for temperature control liquid
Gap for viton gasket
Inset incl. window membrane and liquid channel

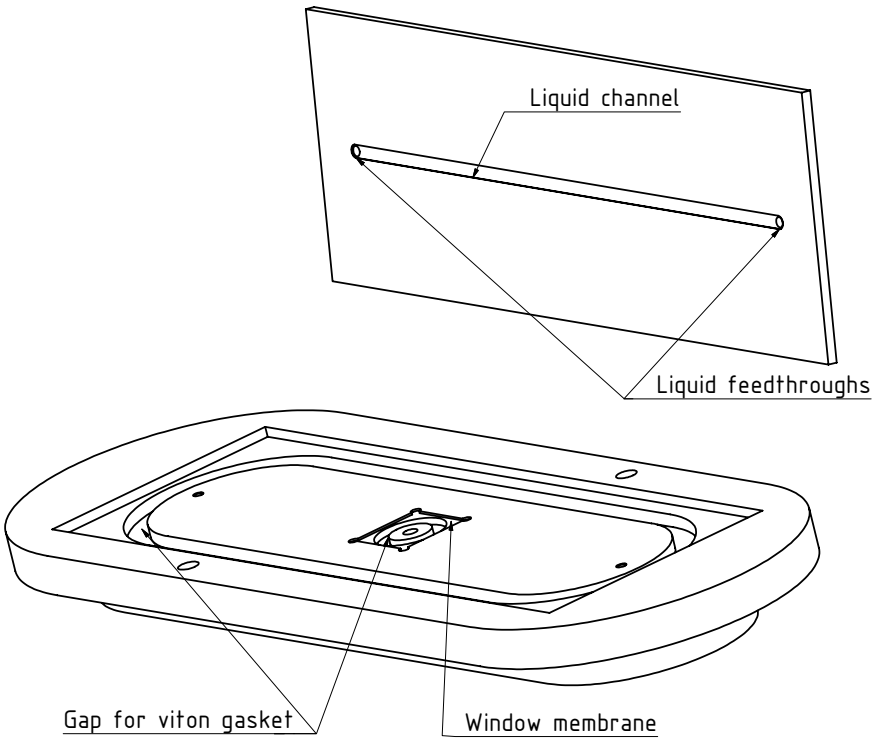
Liquid channel
Liquid feedthroughs
Gap for viton gasket
Window membrane

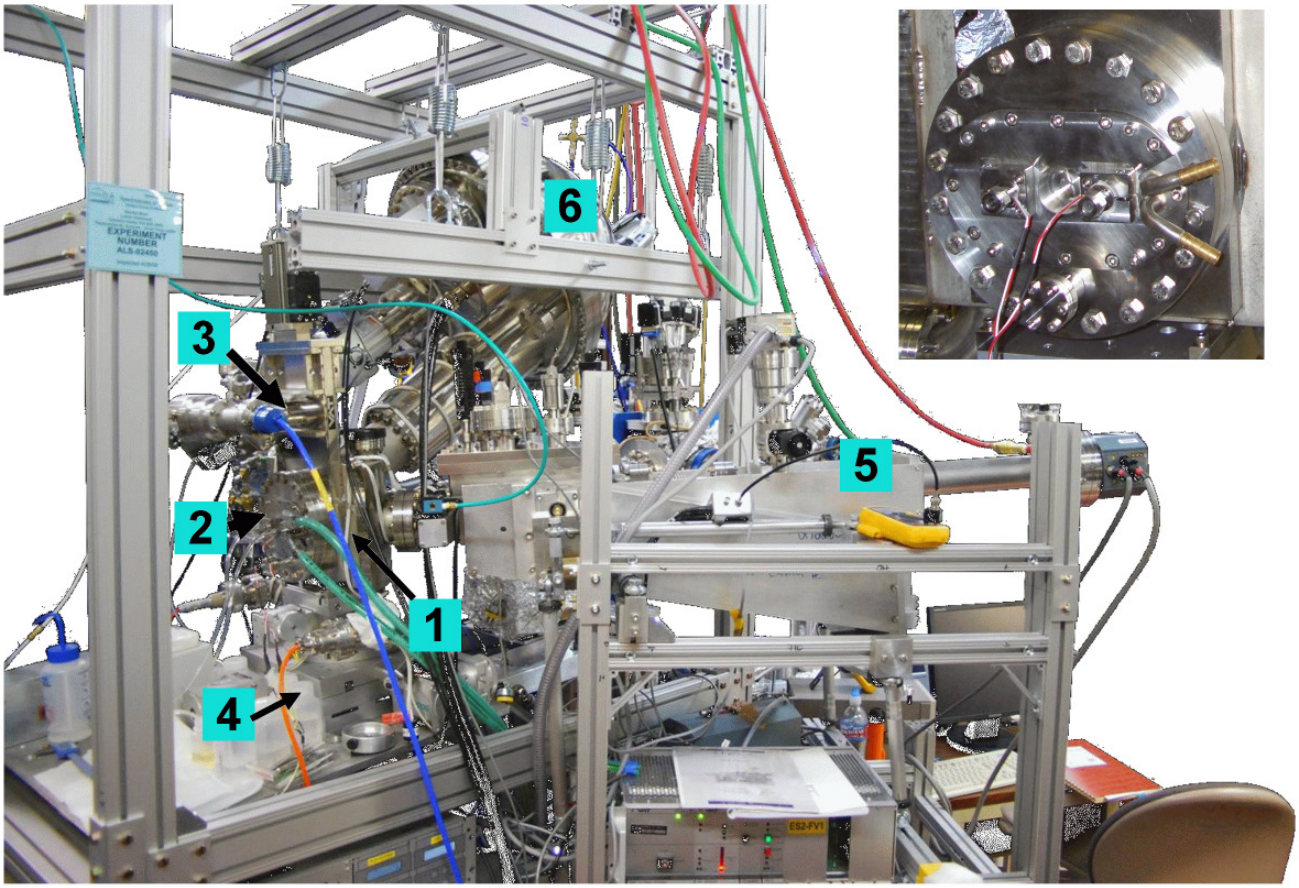
6
3
5
2
1
4

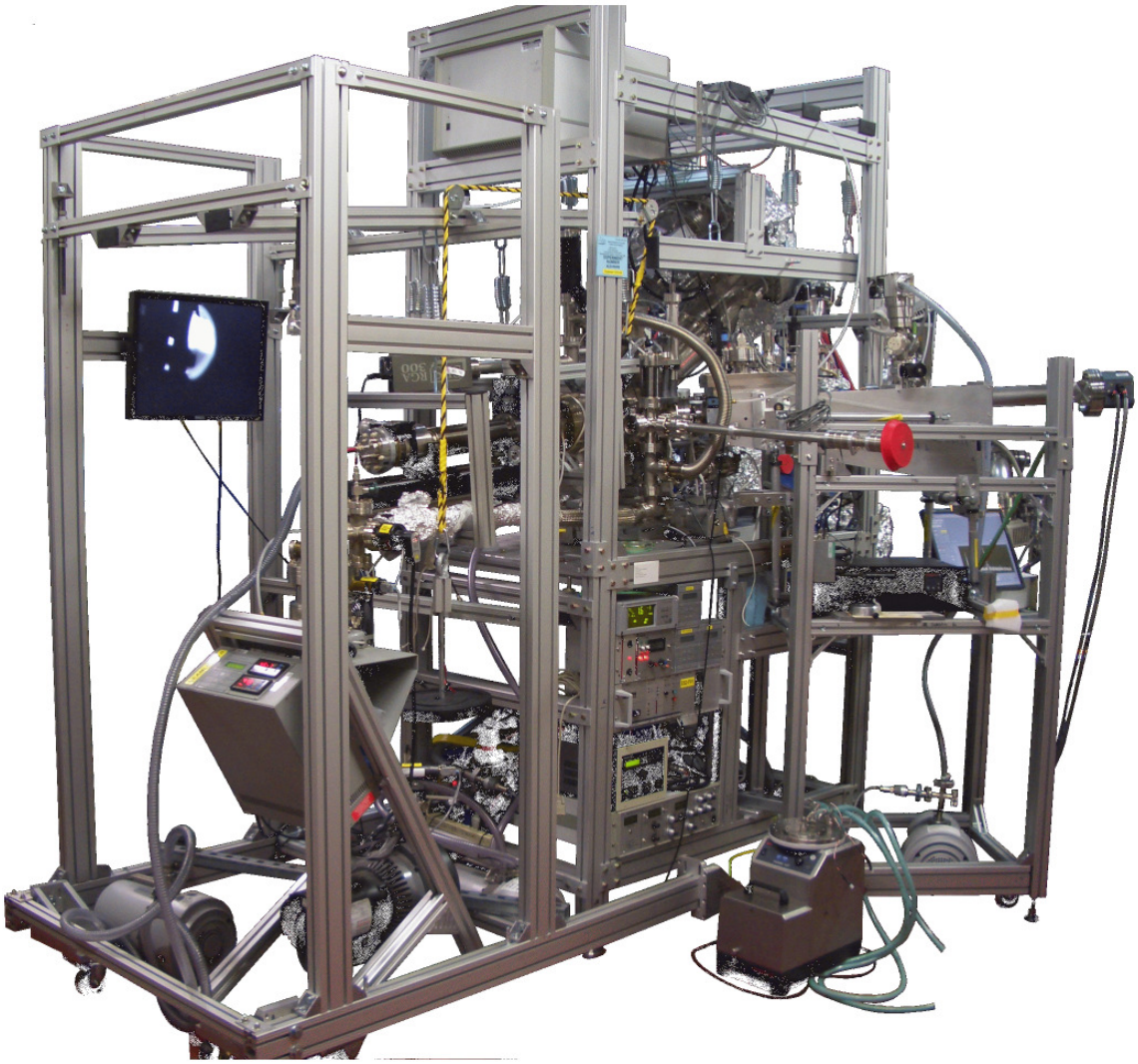

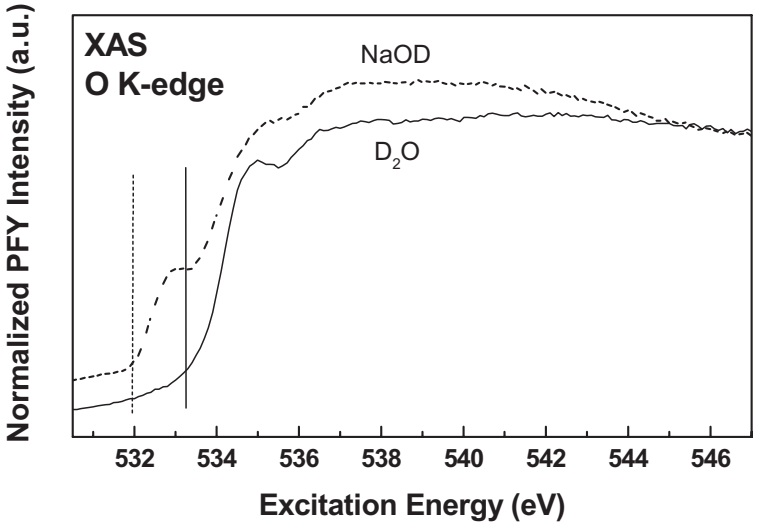
XAS
O K-edge
NaOD
D2O
Normalized PFY Intensity (a.u.)
532
534
536
538
540
542
544
546
Excitation Energy (eV)

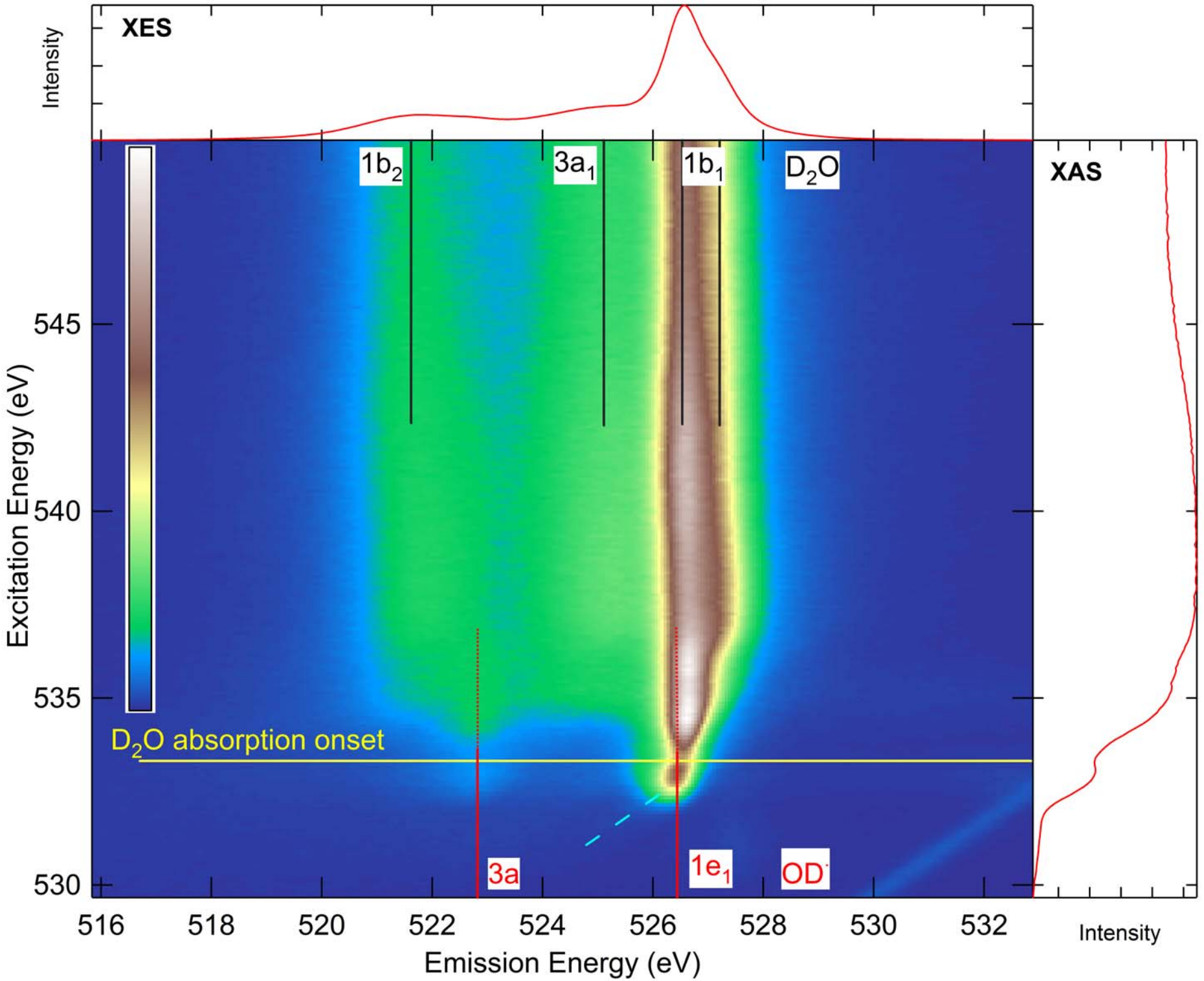
XES
Intensity
1b2
3a1
1b1
D2O
XAS
545
540
535
530
Excitation Energy (eV)
D2O absorption onset
3a
1e1
OD
516
518
520
522
524
526
528
530
532
Emission Energy (eV)
Intensity

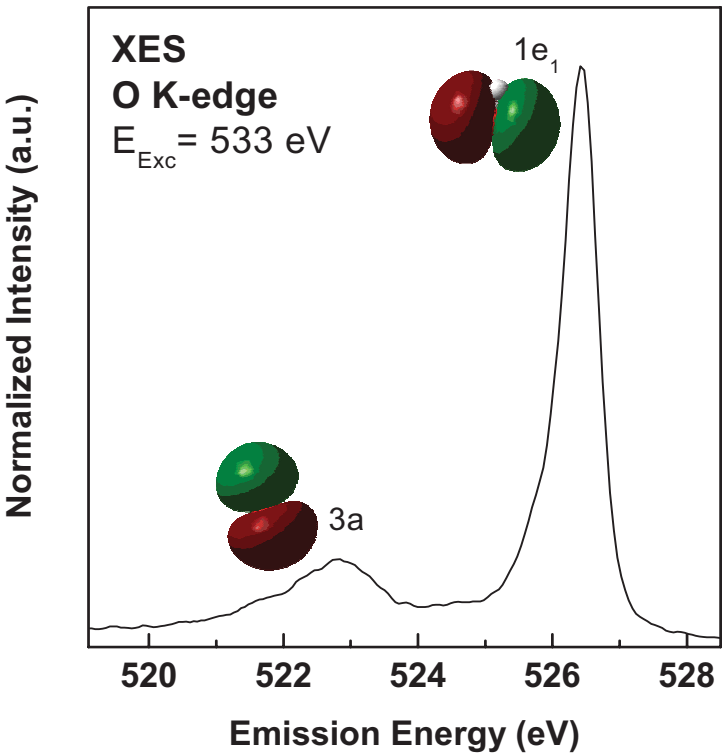
XES
O K-edge
E_Exc = 533 eV
1e1
3a
Normalized Intensity (a.u.)
520
522
524
526
528
Emission Energy (eV)